Autopsy series of 68 cases dying before and during the 1918 influenza pandemic peak

Zong-Mei Sheng[a], Daniel S. Chertow[a], Xavier Ambroggio[b], Sherman McCall[c], Ronald M. Przygodzki[d], Robert E. Cunningham[e], Olga A. Maximova[f], John C. Kash[a], David M. Morens[g], and Jeffery K. Taubenberger[a,1]

[a]Viral Pathogenesis and Evolution Section, Laboratory of Infectious Diseases, [b]Bioinformatics and Computational Biosciences Branch, [f]Office of the Chief, Laboratory of Infectious Diseases, and [g]Office of the Director, National Institute of Allergy and Infectious Diseases, National Institutes of Health, Bethesda, MD 20892; [c]Clinical Pathology Laboratory, US Army Medical Research Institute of Infectious Diseases, Fort Detrick, MD 21702; [d]Department of Veterans Affairs, Washington, DC 20420; and [e]Department of Biophysics, Armed Forces Institute of Pathology, Rockville, MD 20850

Edited* by Robert G. Webster, St. Jude Children's Research Hospital, Memphis, TN, and approved August 16, 2011 (received for review July 11, 2011)

The 1918 to 1919 "Spanish" influenza pandemic virus killed up to 50 million people. We report here clinical, pathological, bacteriological, and virological findings in 68 fatal American influenza/pneumonia military patients dying between May and October of 1918, a period that includes ∼4 mo before the 1918 pandemic was recognized, and 2 mo (September–October 1918) during which it appeared and peaked. The lung tissues of 37 of these cases were positive for influenza viral antigens or viral RNA, including four from the prepandemic period (May–August). The prepandemic and pandemic peak cases were indistinguishable clinically and pathologically. All 68 cases had histological evidence of bacterial pneumonia, and 94% showed abundant bacteria on Gram stain. Sequence analysis of the viral hemagglutinin receptor-binding domain performed on RNA from 13 cases suggested a trend from a more "avian-like" viral receptor specificity with G222 in prepandemic cases to a more "human-like" specificity associated with D222 in pandemic peak cases. Viral antigen distribution in the respiratory tree, however, was not apparently different between prepandemic and pandemic peak cases, or between infections with viruses bearing different receptor-binding polymorphisms. The 1918 pandemic virus was circulating for at least 4 mo in the United States before it was recognized epidemiologically in September 1918. The causes of the unusually high mortality in the 1918 pandemic were not explained by the pathological and virological parameters examined. These findings have important implications for understanding the origins and evolution of pandemic influenza viruses.

archaevirology | postmortem | immunohistochemistry

The 1918 "Spanish" influenza pandemic killed ∼50 million people (1). Archaevirological sequence determination (2–8) and viral reconstruction make it possible to study structure and in vivo pathogenicity of the 1918 pandemic virus (9–21). The origin of the 1918 virus, how and where it evolved before global pandemic spread, and the mechanisms by which this virus caused extraordinarily high mortality have not been fully elucidated. We report here clinical, pathological, bacteriological, and virological features in a case series of 68 influenza/pneumonia fatalities with available autopsy material from the National Tissue Repository of the Armed Forces Institute of Pathology (AFIP) (22, 23) obtained during the period March 1, 1918 to February 28, 1919, a period that includes ∼4 mo before the pandemic was recognized, and 2 mo (September and October 1918) during which it appeared and peaked. This study is unique in demonstrating that the 1918 influenza pandemic virus was circulating and causing fatalities at least 4 mo prior to the pandemic being detected and recognized.

Results

Study Patients. All postmortem examinations with available formalin-fixed, paraffin-embedded (FFPE) lung-tissue blocks were examined (Table S1). The 68 soldiers were all men stationed in US Army training camps, located in the continental US. Medical records indicating date and location of death were available for 59 of 68 cases (87%). The 68 deaths occurred between May 11, 1918 and October 24, 1918 (Fig. 1). Nine of these deaths occurred between May 11 and August 8, 1918, a prepandemic time period with little reported influenza activity in the United States (24). The remaining 59 deaths occurred during the pandemic peak (25), between September 14 and October 24, 1918. Exact date of death was not recorded for 9 of these 59 cases, but their accession numbers indicate that death occurred between September 22 and October 24, 1918 (Table S1).

Clinical Data. Thirty-five of the 59 cases with available medical record information had been diagnosed as having either "influenza and pneumonia" (20 cases) or "influenza and bronchopneumonia" (15 cases). The remaining 24 cases, including all 9 prepandemic cases, had been diagnosed as having either "pneumonia" or "bronchopneumonia" (consistent with diagnosis of influenza in that era). The median age of cases was 27 y (range 18–32 y) and median weight 63.5 kg. Presenting signs and symptoms, available for 56 of 68 cases (82.4%) (Table S2), were typical of influenza, as seen in seasonal and pandemic influenza outbreaks of the era, as well as today (26).

Histopathology. A spectrum of asynchronous histopathological changes was similar in these 68 cases (Figs. 2–5, Table 1, and Table S1), and included bronchitis, bronchiolitis, features of primary influenza viral pneumonia with diffuse alveolar damage [ranging from acute, proliferative, to chronic phases (27)], and evidence of pulmonary repair and remodeling. All 68 cases had additional histological evidence of severe acute bacterial pneumonia (Fig. 2 *A* and *B*), either as the predominant pathology or in conjunction with underlying histopathological features of influenza viral infection (Fig. 2 *C* and *D*, Table 2, and Table S1). Bacterial pneumonic changes ranged from focal to extensive in distribution and were usually associated with visible bacteria on tissue Gram stain (Fig. 3). The histopathological spectrum corresponded to the typical pathology of bacterial pneumonia (e.g., marked pulmonary infiltration by neutrophils in pneumococcal pneumonia and multiple microabscesses with marked neutrophilic infiltration in staphylococcal pneumonia) (28). Acute bacterial pleuritis was observed in 15% of the cases (Table 1).

Author contributions: J.K.T. designed research; Z.-M.S., D.S.C., X.A., S.M., R.M.P., R.E.C., O.A.M., J.C.K., and J.K.T. performed research; X.A. and O.A.M. contributed new reagents/analytic tools; Z.-M.S., D.S.C., X.A., J.C.K., D.M.M., and J.K.T. analyzed data; and J.K.T. wrote the paper.

The authors declare no conflict of interest.

*This Direct Submission article had a prearranged editor.

Data deposition: The sequences reported in this paper have been deposited in the GenBank database (accession no. JN620390–JN620401).

[1]To whom correspondence should be addressed. E-mail: taubenbergerj@niaid.nih.gov.

This article contains supporting information online at www.pnas.org/lookup/suppl/doi:10.1073/pnas.1111179108/-/DCSupplemental.

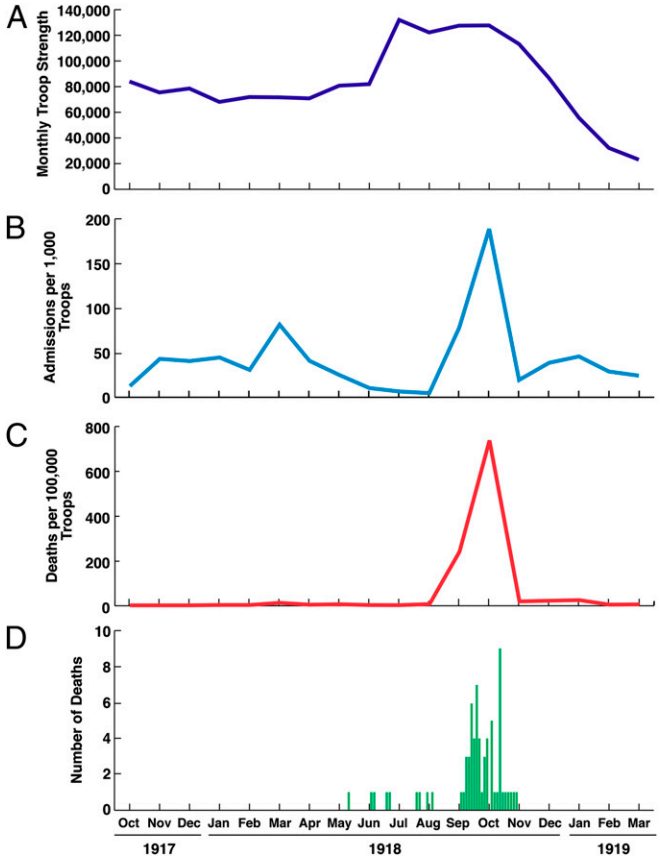

Fig. 1. Troop strength, monthly admissions for, and deaths from, influenza or pneumonia of nonindicated cause at seven United States military training camps, October 1917 to March 1919. The camps include Camp Dodge, Johnston, IA; Camp Funston, Manhattan, KS; Camp Green, Charlotte, NC; Camp Jackson, Columbia, SC; Camp Lee, Petersburg, VA; Camp Travis, San Antonio, TX; and Camp Upton, Yaphank, NY. Data from Walter Reed Hospital, Washington, DC, were not available. Troop-strength data include all officers and enlisted men. Monthly admission and death data by camp were only available for enlisted men. Separate data for "white" and "colored" enlisted men were combined. (*A*) Number of United States troops by month. (*B*) Number of admissions for influenza-like illness per 1,000 troops by month. (*C*) Number of deaths from influenza or pneumonia per 100,000 troops by month. (*D*) Date of death of the 68 cases in the 1918 autopsy series included in this study.

These pathological findings were correlated with postmortem bacterial lung culture results that had been recorded for 44 of 68 cases in 1918 (Table S1). Two of the 44 cultures had been recorded as unsatisfactory; 40 of the remaining 42 (95.2%) grew one or more pneumopathogenic bacteria (Table 2). Tissue Gram stains performed on slides recut in 2011 were positive for bacteria in 63 of 67 cases examined (94%), often with abundant visible bacteria, each of these associated with histologic features of acute bacterial pneumonia. The majority of these were Gram-positive and morphologically compatible with either *Streptococcus pneumoniae*, *Streptococcus pyogenes*, or *Staphlyococcus aureus*, concordant with the 1918 lung culture results (Table S1).

Detection of Influenza Viral RNA and Antigens. Influenza infection was detected in 37 of the 68 cases (54%) by the presence of either viral antigens or RNA. Control staining for cytokeratins AE1 and AE3, performed following antigen retrieval, was positive in respiratory epithelial cells in 47 of 49 cases (96%) tested, indicating well-preserved general tissue immunoreactivity 93 y after fixation.

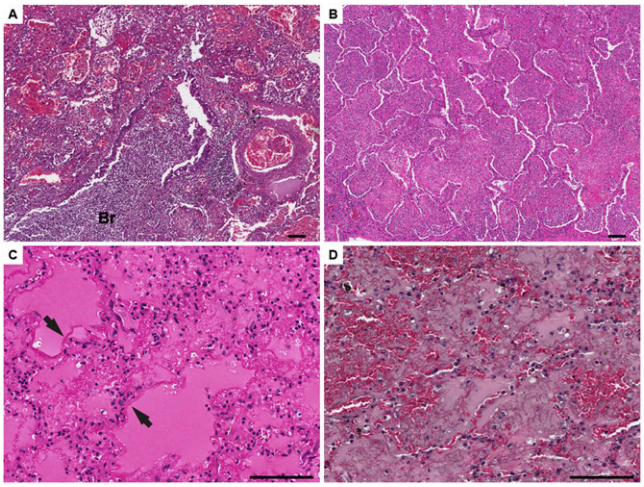

Fig. 2. Representative histopathological changes associated with fatal 1918 influenza and pneumonia cases. Photomicrographs of H&E-stained sections are shown. (*A*) Section of lung with acute pneumonia, showing a bacterial bronchopneumonic pattern consisting of massive infiltration of neutrophils into the lumen of a bronchiole (Br) and into the airspaces of the surrounding alveoli (pandemic peak case 19181008e). (*B*) Section of lung with acute bacterial pneumonia as in *A*, showing massive infiltration of neutrophils in the airspaces of the alveoli (pandemic peak case 19181008g). (*C*) Section of lung showing DAD with hyaline membranes lining alveoli (arrows). The alveolar airspaces contain edema fluid, strands of fibrin, desquamated epithelial cells, and inflammatory cells (pandemic peak case 19181007). (*D*) Section of lung showing pulmonary hemorrhage. The alveolar airspaces contain erythrocytes, edema fluid, strands of fibrin, desquamated epithelial cells, and inflammatory cells (pandemic peak case 19180922a). (Scale bars, 100 μm.)

Influenza virus antigens were detected in 33 of 67 (51%) tissues (Figs. 4 and 5, and Table S1).

Viral antigen distribution ranged from focal to multifocal, and was similar in all positive cases, including those dying in the prepandemic and in the pandemic peak periods. Staining of pseudostratified columnar epithelium of the respiratory tree, including bronchial (Fig. 4*A*) and bronchiolar epithelium (Fig. 4*B*), and associated bronchial submucosal glands (Fig. 4*A*) was prominent. Viral antigens were detected predominantly in the luminal, rather than the basal epithelial cells (compare Fig. 4*B*, showing viral antigens, and Fig. 4*D*, showing cytokeratins in adjacent sections of one bronchiole). Viral antigens were observed in both ciliated cells and mucus cells.

Influenza viral bronchitis was observed in all cases for which bronchial tissue sections were available, consisting of denuded and ulcerated epithelial layers, focal squamous metaplasia, and submucosal inflammatory infiltration, compatible with previous reports (29, 30). Viral infection extended into the submucosal

Table 1. Major pulmonary histological diagnoses

Characteristic	No./total no. (%)
Bronchitis	4/4* (100%)
Acute pneumonia	68/68 (100%)
Bronchiolitis	39/68 (57%)
DAD	36/68 (53%)
Acute edema	41/68 (60%)
Acute hemorrhage	27/68 (40%)
Thrombus formation	5/68† (7%)
Pleuritis	10/68 (15%)

*Only 4 of 68 cases had evaluable bronchial tissue.
†One patient with thrombus formation has recently been reported as bearing sickle-cell trait (52).

Table 2. Postmortem bacterial lung culture results in 1918

1918 culture result (current preferred nomenclature)	No./total (%)
Pneumococcus (*Streptococcus pneumonia*)	22/42 (52.4)
Pneumococcus, Serotype I	2/42 (4.8)
Pneumococcus, Serotype II	5/42 (11.9)
Pneumococcus, Serotype III	7/42 (16.7)
Pneumococcus, Serotype IV*	5/42 (11.9)
Pneumococcus, not serotyped	3/42 (7.1)
Streptococcus, hemolytic (*Streptococcus pyogenes*)	4/42 (9.5)
Streptococcus, nonhemolytic	1/42 (2.4)
Staphylococcus	4/42 (9.5)
Friedländler's bacillus (*Klebsiella pneumonia*)	1/42 (2.4)
Bacillus coli (*Escherichia coli*)	1/42 (2.4)
Diplococci observed in sections	1/42 (2.4)
Mixed cultures	6/42 (14.3)
Pneumococcus + *Streptococcus*	2/42 (4.8)
Pneumococcus + *Staphylococcus*	1/42 (2.4)
Streptococcus + *Staphylococcus*	2/42 (4.8)
Pneumococcus + *Staphylococcus* + Friedländler's bacillus	1/42 (2.4)
Negative	2/42 (4.8)

*Serotype IV in 1918 included a number of polysaccharide capsular types that were subsequently assigned to newly identified types (43).

glands and ducts as moderate-to-marked inflammation with focal epithelial cytonecrosis (Fig. 4*A*). Focal mild-to-severe bronchiolitis was observed in 39 of 68 cases (57%), 28 of which (72%) also had viral antigens in the bronchiolar respiratory epithelium (Fig. 4*B*).

Influenza viral pneumonia with focal-to-extensive diffuse alveolar damage (DAD) was seen in 42 of 68 cases (62%) (Figs. 2 *C* and *D*, and 4*C*), often in association with marked pulmonary edema (41 of 68 cases, 60%), hyaline membrane formation (9 of 68 cases, 13%) (Fig. 2*C*), and acute pulmonary hemorrhage (27 of 68 cases, 40%) (Fig. 2*D*). Influenza viral antigen was located in alveolar lining cells (Fig. 5 *C* and *D*), morphologically compatible both with type I and type II cells, and in the apical cells of the bronchiolar respiratory epithelium (Fig. 5 *E* and *F*) in patterns indistinguishable between cases. Influenza viral antigen was detected focally-to-multifocally in both the cytoplasm and nuclei of alveolar macrophages and alveolar epithelial cells (Fig. 5 *B–D*), with no apparent differences between cases from the prepandemic and pandemic peak periods, or in cases associated with viruses having different apparent receptor-binding specificities (31, 32) (see below). Influenza antigen was also detected focally in hyaline membrane material, suggesting persistence of viral antigens well into the later stages of acute lung injury, as seen in the 2009 H1N1 influenza pandemic (33).

Influenza virus RNA was detected by RT-PCR in a subset of 13 of 21 (61%) cases tested (Table S1) (see *Materials and Methods*). Partial HA1 domain sequences encoding the principal amino acids of the viral receptor-binding domain (RBD) (31, 34) were determined in 11 of these cases (Table S3), providing additional data for comparison with viral sequences previously reported (2, 3, 35). Three of four HA1 domain sequences from the prepandemic cases shared the RBD sequence configuration of viruses from two previously reported cases (2, 3, 35), having a mixed α2-3 SA ("avian-like:) and α2-6 SA ("human-like") glycan binding specificity (Table S3). Seven of nine sequences from pandemic peak cases, and two of three sequences from postpeak cases [as published previously (2, 3, 35)] had the RBD sequence configuration associated with α2-6 SA glycan binding. All sixteen available 1918 virus HA1 sequences possess an 187D change from the avian influenza A virus HA consensus, associated with a switch to α2-6 SA glycan binding in HAs of the H1 subtype. As noted, there were no

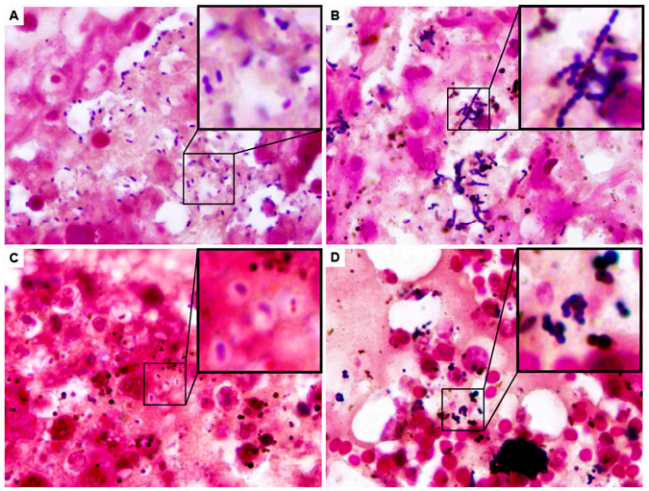

Fig. 3. Tissue Gram stains of fatal 1918 influenza and pneumonia cases. (*A*) Gram-positive diplococci morphologically compatible with *S. pneumoniae* (prepandemic peak case 19180603 with lung culture in 1918 positive for pneumococcus and *Staphylococcus*). (*B*) Gram-positive cocci in chains morphologically compatible with *S. pyogenes* (pandemic peak case 19181008c with no available 1918 lung culture information). (*C*) Gram-positive diplococci morphologically compatible with *S. pneumoniae* with prominent capsules (see *Inset*) (pandemic peak case 19180924d with lung culture in 1918 positive for pneumococcus, type II). (*D*) Gram-positive cocci morphologically compatible with *S. aureus* (pandemic peak case 19180921 with lung culture in 1918 positive for *S. aureus*). Magnification 1,000×; *Insets* show higher power magnification of boxed areas in *A–D*.

apparent differences in histopathology or viral antigen distribution between cases with the G222 (mixed α2-3 SA/α2-6 SA) or D222 (α2-6 SA) polymorphism, or between prepandemic peak and pandemic peak cases.

Other than the residue 222 polymorphism, 1918 viral sequences were highly conserved in this region of the HA1 domain. One of the pandemic peak cases with D222, however, also possessed a novel Q189R change near the RBD (Table S3). To assess whether this unique polymorphism might alter receptor-binding specificity, computational docking simulations were performed with a modeled HA1 Q189R variant and a human receptor (α2-6 SA) sialo-pentasaccharide analog LSTc. In the predicted complexes, LSTc was found to adopt the folded conformation associated with the α2-6 linkage, placing the carbohydrate moieties distal to the sialic acid across the N-terminal portion of the RBD 190-helix in close proximity to position 189 (Fig. S1). Viral antigen immunostaining from this case shows focal positivity in bronchiolar epithelial cells apparently identical to the staining patterns observed in the other cases.

Discussion

The place and time of origin of the 1918 influenza pandemic virus is unknown, with no evidence of excess respiratory disease or of excess mortality detected in United States military camps from May through September 1918 (36) (Fig. 1). As would be expected based on the explosive United States pandemic outbreak later in the fall, the pandemic influenza virus must nevertheless have been circulating silently—and causing occasional fatalities—at least 4 mo before the pandemic was first detected in the United States. The lack of detectable disease and mortality in the prepandemic months is consistent with a virus, perhaps imported from abroad (37), needing time to spread from one individual case to another and thereby gradually reach a threshold of epidemiological detection. With a speculative serial generation time of 4.5 d (38), basic reproductive rate of 1.8 (39), and case-fatality ratio probably no higher than 1% to 2% in the summer months, it would clearly

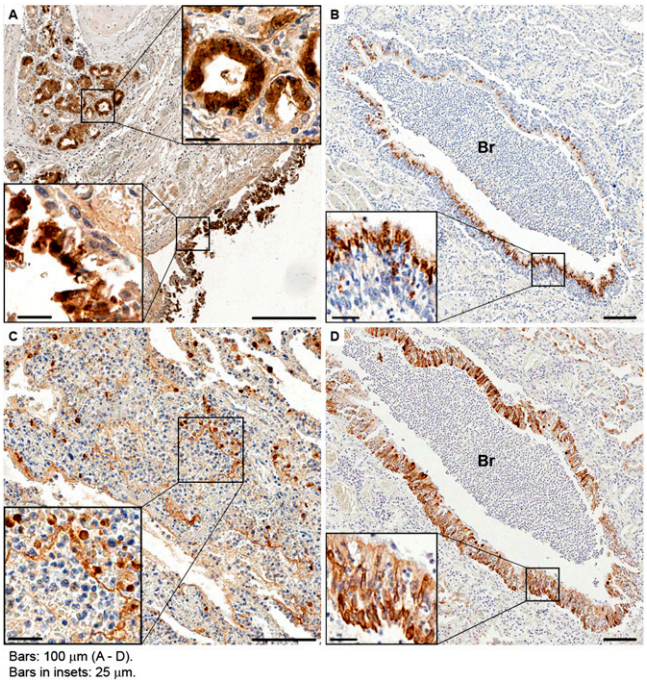

Fig. 4. Immunohistochemical analyses of fatal 1918 influenza and pneumonia cases. Photomicrographs of anticytokeratin- and anti-influenza–stained sections are shown. Influenza viral antigen (*A*–*C*) or cytokeratins (*D*) are stained reddish-brown on a hematoxylin-stained background. (*A*) Acute and necrotizing influenza viral bronchitis with infection of the submucosal mucus glands. Influenza viral antigen is readily apparent in the overlying bronchial epithelium (*Inset*, *Lower Left*) and in the acinar cells of the submucosal bronchial glands (*Inset*, *Upper Right*) (pandemic peak case 19180930b). (*B*) Acute influenza viral bronchiolitis with infiltration of neutrophils and other inflammatory cells in the lumen of a bronchiole (Br). Influenza viral antigen is readily apparent in the apical cells of the bronchiolar respiratory epithelium (see *Inset*), (prepandemic peak case 19180602). (*C*) Influenza viral antigen staining in alveolar epithelial cells and alveolar macrophages (pandemic peak case 19180930b). (*Inset*) Prominent alveolar antigen staining in the epithelium lining an alveolus and in alveolar macrophages. (*D*) Acute influenza viral bronchiolitis with infiltration of neutrophils and other inflammatory cells in the lumen of a bronchiole (Br). Cytokeratin staining is readily apparent in the full thickness of the bronchiolar respiratory epithelium, including basal epithelial cells (*Inset*). Cytokeratin staining of alveolar epithelial cells is also apparent in the top right of the figure (prepandemic peak case 19180602, serial section of same block as *B*). Scale bars in *A*–*D*, 100 μm; bars in *Insets*, 50 μm.

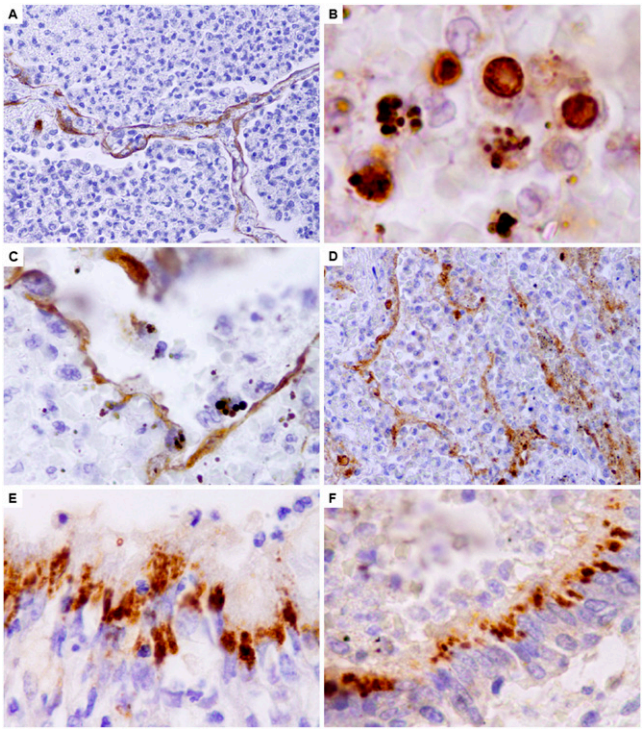

Fig. 5. Immunohistochemical analyses of fatal 1918 influenza and pneumonia cases. Photomicrographs of anticytokeratin- and anti-influenza–stained sections are shown. Cytokeratins (*A*) or influenza viral antigen (*B*–*F*) are stained reddish-brown on a hematoxylin-stained background. (*A*) Alveolar epithelial cells stained for control cytokeratins AE1& AE3 in case 19181001a. (*B*) Alveolar macrophages in pandemic peak case 19180924d with both cytoplasmic and prominent nuclear staining. (*C*) Alveolar epithelial cells stained for influenza viral antigen in case 19180924d, with RBD polymorphism G222 (Table S3). (*D*) Alveolar epithelial cells stained for influenza viral antigen in pandemic peak case 19180930b, with RBD polymorphism D222 (Table S3). (*E*) Bronchiolar respiratory epithelial cells stained for influenza viral antigen in prepandemic peak case 19180602 with RBD polymorphism G222 (Table S3) (original magnification 1,000×). (*F*) Bronchiolar respiratory epithelial cells stained for influenza viral antigen in pandemic peak case 19181001e with RBD polymorphism D222 (Table S3) Original magnification 400× (*A* and *D*); 1,000× (*B*, *C*, *E*, and *F*).

take weeks, even under favorable circumstances, for an imported "founding virus" to produce enough cases for a small outbreak to occur or for fatalities to be detected statistically.

For unknown reasons, summer (Northern Hemisphere) spread of newly introduced pandemic influenza viruses has historically (e.g., 1580, 1782) and more recently (e.g., 1957, 1968, and 2009) been indolent (40). In this respect, it is noteworthy that mortality peaks associated with respiratory disease had occurred in a few Northern European countries in July to August 1918 (37). This finding is consistent with the possibility that the pandemic virus had relative difficulty gaining a foothold in Europe during the unfavorable summer months, assuming that—as long believed—elevated temperature and humidity may hinder pandemic influenza virus transmission in all but the coolest, driest climates (41, 42). Moreover, independent of transmission, summer influenza mortality and case-fatality are usually lower than in the winter (40), when primary and secondary bacterial pneumonias are more highly incident (43).

Determination of RBD sequences from fatal prepandemic and pandemic peak cases, as a function of time of viral circulation, adds to information on critical viral binding sites associated with cell attachment. Three of the four prepandemic (May–August 1918) strain sequences have the G222 RBD configuration associated with mixed α2-3 SA/α2-6 SA receptor binding, whereas seven of the nine pandemic peak—and two of the three postpeak strain sequences—have the D222 configuration associated with α2-6 SA binding (31, 32, 35) (Table S3).

Among several possibilities, the pandemic virus could have been evolving toward more efficient transmissibility in the earlier periods of circulation in human populations, consistent with decreased ferret transmissibility of a 1918 virus containing the G222 versus the D222 configuration (15). However, this possibility is difficult to reconcile with calculated high transmissibility rates in prepandemic (July–August 1918) cases in Northern Europe compared with pandemic peak cases (37), or retention of the G222 configuration in viruses detected as late as February 1919 (35). Moreover, the high percentage of 1918-descended seasonal H1N1 viruses of recent decades that bear G222 (with or without Q189R) is also problematic. That the G222 residue sits on one edge of the RBD (44) and is included in one of the major H1 antigenic domains of Ca_2 (45) suggests an alternative possibility: that increasing frequency of D222 during pandemic progression could reflect antigenic drift pressure from growing population immunity (35). The

differences at the 222 site might also represent different modes of transmission (e.g., droplet inoculation versus aerosol) associated with different climatological conditions (46), infective tropism for different cells at varying levels of the respiratory tree, preferential selection of variants from a transmitted quasispecies, the effect of a founding virus, or of statistical chance.

In any case, we did not observe apparent differences in the cellular distribution of viral antigens in 1918 cases for which sequence confirmation indicates either the G222 or D222 polymorphism (Fig. 5 and Table S3). This finding suggests that despite significantly different binding specificities in vitro (31, 47), at terminal stages of infection 1918 strains with G222 and D222 RBD polymorphisms had the same cellular tropism along the human respiratory epithelial tree. This finding is also in accord with mouse and ferret studies, indicating that cellular tropism of 1918 influenza viruses bearing the α2-6 SA or the mixed α2-3 SA/α2-6 SA binding preference did not affect pathogenicity, and that viral antigen distribution was not different immunohistochemically (15, 17). In future work, it might be possible to perform dual labeling for influenza viral antigens and cell-type specific markers. It has also recently been suggested that 2009 H1N1 strains with 222G, which constitute a minority of isolates, are associated with more severe illness (48), but the biological and clinical significance of these observations is not yet known.

Although the biological significance of the 1918 viral RBD polymorphisms observed also remains unclear, structural analysis of the novel Q189R polymorphism in one pandemic peak virus indicates that the substitution may enhance α2-6 SA binding. Computational modeling simulations predict RDB-receptor complexes in which the guanidinium group of R189 contacts human SA-receptor analogs through hydrogen bonds with the axial hydroxyls of the carbohydrate moiety in the fifth position. In contrast, Q189 is not found to interact with LSTc, and to our knowledge this position has not been observed experimentally (31, 32, 34) or through extensive molecular dynamic simulations with other HA subtypes (49) to make significant contacts with human receptors. In the predicted complexes, the Q189R side chain is remote from receptor-binding interactions that have been proposed to be important for binding receptors with α2-3 linkages. This finding suggests the experimentally testable hypothesis that the R189 substitution in H1 may result in increased binding affinities of α2-6 SA receptors without significantly effecting α2-3 SA receptor-binding affinities. It is of note that R189 was frequently observed in H1N1 seasonal influenza isolates in the 1980s to 2000s.

The data from this case series confirm that the clinical course and postmortem histopathological and microbiological findings in fatal 1918 pandemic influenza infections are not unique (29), and provide further evidence for the importance of secondary/concurrent bacterial pneumonias in fatal outcomes. The microbiological data presented here support previous studies (reviewed in ref. 43) suggesting that fatal bacterial pneumonias in 1918 were associated with different bacteria, but most commonly pneumopathogenic Gram-positive organisms. In future work it may be possible to further characterize the bacteria present by molecular genetic analyses.

The cellular distribution of influenza viral antigens in this series of fatal 1918 cases, uniquely examined here, is remarkably similar to that observed in fatal 2009 pH1N1 pneumonia cases (33). As with the 2009 pandemic, immunohistochemical evidence of ongoing influenza virus infection is present in these fatal cases dying on average 9 d after clinical onset. The data show prominent viral infection of the pseudostratified columnar epithelium of the respiratory tree, extending from bronchi to bronchioles (29), with focal infection of alveolar epithelial cells and alveolar macrophages. Detection of influenza virus antigens in the nuclei of all these cell types confirms active viral replication. As seen in both the 1918 and 2009 pandemics, evidence of repair, including alveolar type II hyperplasia and organizing fibrosis, was common (33).

Consistent with in vitro data on apical influenza viral budding in polarized cells (50), detection of 1918 influenza viral antigens in the luminal (apical) cells of the respiratory epithelium of bronchioles (Fig. 4*B*) suggests that viral budding and spread progresses apically rather than basolaterally, consistent with viral spread by direct extension down the respiratory tree (43). Similar viral antigen staining patterns were observed in postmortem examinations of fatal 2009 pandemic influenza virus cases (33), and in experimental 1918 virus infections of macaques (14). Although an autopsy series cannot delineate the natural history of infection and disease, the pathological data appear to be consistent with a primary viral panbronchial and bronchiolar infection together with primary viral pneumonia (characterized predominantly by diffuse alveolar damage), which may create an opportunity, through mechanisms not yet fully understood, for pneumopathogenic bacteria carried in the nasopharynx to gain access to the lung and cause severe and fatal secondary bacterial pneumonias (with massive alveolar infiltration of neutrophils). Data from the case series do not support the hypothesis that high mortality in the 1918 pandemic resulted from unique pathogenic mechanisms, such as increased cytopathicity, basolateral budding, or altered cell tropism and viral distribution. The data cannot, however, rule out effects of pathogenic host immune responses, of more rapid or higher titer viral growth, or of other important but unknown host or environmental cofactors.

In summary, the 1918 pandemic influenza virus circulated silently in the United States for at least 4 mo before the pandemic was first detected in late September to October 1918. Based on a small number of HA1 receptor-binding domain sequences, early prepandemic circulation may have been associated with viral variants bearing a G222 RBD configuration, often described as "avian-like" on the basis of in vitro binding studies. The significance of this finding, if any, is unknown. Prepandemic, pandemic peak, and postpandemic viruses all caused fatalities associated with the same apparent clinical and pathological features of panbronchitis, bronchiolitis, and diffuse alveolar damage associated with early focal repair, but complicated by severe secondary bacterial pneumonia. This pathology is indistinguishable from that of influenza deaths in subsequent pandemics, including the 2009 H1N1 pandemic, and in seasonal influenza deaths (28, 29, 33), and may suggest a common pathway to severe and fatal outcomes associated with many or most human-adapted influenza viruses. The high number of influenza deaths in 1918 has led in recent years to the widespread speculation about unusual viral virulence properties, supported by experimental animal studies (12, 13), but in its disease course and clinicopathologic features the 1918 pandemic was different in degree, but not in kind, from previous and subsequent pandemics (25). Despite the extraordinary number of global deaths, the vast majority of influenza cases in 1918 (>97% in industrialized nations) were self-limited and essentially indistinguishable from influenza cases today (36). Additionally, influenza severity and death in 1918 to 1919 correlated with the frequency of well-understood secondary bacterial pneumonias caused by common pneumopathogens (43). The cause of extraordinarily high mortality in the 1918 pandemic appears not to be exclusively a factor of viral virulence, and thus remains to be more fully elucidated (13, 14).

Materials and Methods

Patients. All available postmortem cases from United States soldiers dying of probable influenza between March 1, 1918 and February 28, 1919 were retrieved from the National Tissue Repository of the AFIP under active research protocols of coauthor J.K.T. (3, 8). Sixty-eight cases were analyzed for this study.

Histopathological and Microbiological Studies. Materials examined included the 93-y-old FFPE tissues, stained slides, and clinical records (available in 59 of 68 cases). Five-micrometer thick sections were cut from the available FFPE lung tissue blocks and stained with H&E for histopathological examination, and Brown and Hopps tissue Gram stain for bacteria. For viral antigen im-

munohistochemistry, sections were placed on positively charged glass slides and subjected to heat-induced antigen retrieval in 10 mM sodium citrate buffer, pH 6.0, for 8.5 min.

Molecular Studies. In a subset of 21 cases, RNA was extracted from the FFPE tissue sections for influenza A virus RT-PCR, including quantitative real-time RT-PCR for the influenza A virus matrix 1 gene, as previously described (2, 51), and by RT-PCR for amplicons within the 1918 hemagglutinin (H1 subtype) HA1 domain (primers available on request) (3).

Additional Methods. Detailed descriptions of methods for immunohistochemistry, molecular studies, and molecular modeling are available in *SI Materials and Methods*.

ACKNOWLEDGMENTS. We thank Frank Roberts and the repository staff of the Armed Forces Institute of Pathology for their help in locating 1918 case material, and Jen Hammock for assistance with the histological preparations. This work was supported by the intramural funds of the National Institutes of Health and the National Institute of Allergy and Infectious Diseases.

1. Johnson NP, Mueller J (2002) Updating the accounts: Global mortality of the 1918–1920 "Spanish" influenza pandemic. *Bull Hist Med* 76:105–115.
2. Taubenberger JK, Reid AH, Krafft AE, Bijwaard KE, Fanning TG (1997) Initial genetic characterization of the 1918 "Spanish" influenza virus. *Science* 275:1793–1796.
3. Reid AH, Fanning TG, Hultin JV, Taubenberger JK (1999) Origin and evolution of the 1918 "Spanish" influenza virus hemagglutinin gene. *Proc Natl Acad Sci USA* 96: 1651–1656.
4. Reid AH, Fanning TG, Janczewski TA, Taubenberger JK (2000) Characterization of the 1918 "Spanish" influenza virus neuraminidase gene. *Proc Natl Acad Sci USA* 97: 6785–6790.
5. Basler CF, et al. (2001) Sequence of the 1918 pandemic influenza virus nonstructural gene (NS) segment and characterization of recombinant viruses bearing the 1918 NS genes. *Proc Natl Acad Sci USA* 98:2746–2751.
6. Reid AH, Fanning TG, Janczewski TA, McCall S, Taubenberger JK (2002) Characterization of the 1918 "Spanish" influenza virus matrix gene segment. *J Virol* 76: 10717–10723.
7. Reid AH, Fanning TG, Janczewski TA, Lourens RM, Taubenberger JK (2004) Novel origin of the 1918 pandemic influenza virus nucleoprotein gene. *J Virol* 78:12462–12470.
8. Taubenberger JK, et al. (2005) Characterization of the 1918 influenza virus polymerase genes. *Nature* 437:889–893.
9. Kobasa D, et al. (2004) Enhanced virulence of influenza A viruses with the haemagglutinin of the 1918 pandemic virus. *Nature* 431:703–707.
10. Kash JC, et al. (2004) Global host immune response: Pathogenesis and transcriptional profiling of type A influenza viruses expressing the hemagglutinin and neuraminidase genes from the 1918 pandemic virus. *J Virol* 78:9499–9511.
11. Tumpey TM, et al. (2004) Pathogenicity and immunogenicity of influenza viruses with genes from the 1918 pandemic virus. *Proc Natl Acad Sci USA* 101:3166–3171.
12. Tumpey TM, et al. (2005) Characterization of the reconstructed 1918 Spanish influenza pandemic virus. *Science* 310:77–80.
13. Kash JC, et al. (2006) Genomic analysis of increased host immune and cell death responses induced by 1918 influenza virus. *Nature* 443:578–581.
14. Kobasa D, et al. (2007) Aberrant innate immune response in lethal infection of macaques with the 1918 influenza virus. *Nature* 445:319–323.
15. Tumpey TM, et al. (2007) A two-amino acid change in the hemagglutinin of the 1918 influenza virus abolishes transmission. *Science* 315:655–659.
16. Pappas C, et al. (2008) Single gene reassortants identify a critical role for PB1, HA, and NA in the high virulence of the 1918 pandemic influenza virus. *Proc Natl Acad Sci USA* 105:3064–3069.
17. Qi L, et al. (2009) Role of sialic acid binding specificity of the 1918 influenza virus hemagglutinin protein in virulence and pathogenesis for mice. *J Virol* 83:3754–3761.
18. Weingartl HM, et al. (2009) Experimental infection of pigs with the human 1918 pandemic influenza virus. *J Virol* 83:4287–4296.
19. Watanabe T, et al. (2009) Viral RNA polymerase complex promotes optimal growth of 1918 virus in the lower respiratory tract of ferrets. *Proc Natl Acad Sci USA* 106: 588–592.
20. Van Hoeven N, et al. (2009) Pathogenesis of 1918 pandemic and H5N1 influenza virus infections in a guinea pig model: Antiviral potential of exogenous alpha interferon to reduce virus shedding. *J Virol* 83:2851–2861.
21. Watanabe T, Kawaoka Y (2011) Pathogenesis of the 1918 pandemic influenza virus. *PLoS Pathog* 7:e1001218.
22. Nelson AM, Sledzik PS, Mullick FG (1996) The Army Medical Museum/Armed Forces Institute of Pathology and Emerging Infections: from camp fevers and diarrhea during the American Civil War in the 1860's to global molecular epidemiology and pathology in the 1990s. *Arch Pathol Lab Med* 120:129–133.
23. Krafft AE, Duncan BW, Bijwaard KE, Taubenberger JK, Lichy JH (1997) Optimization of the isolation and amplification of RNA from formalin-fixed, paraffin-embedded tissue: The Armed Forces Institute of Pathology experience and literature review. *Mol Diagn* 2:217–230.
24. Hall MW (1928) Inflammatory diseases of the respiratory tract (bronchitis; influenza; bronchopneumonia; lobar pneumonia). *The Medical Department of the United States Army in the World War*, eds Ireland MW, Siler JF (U.S. Government Printing Office, Washington, DC), Vol IX, pp 61–169.
25. Taubenberger JK, Morens DM (2006) 1918 Influenza: The mother of all pandemics. *Emerg Infect Dis* 12:15–22.
26. Call SA, Vollenweider MA, Hornung CA, Simel DL, McKinney WP (2005) Does this patient have influenza? *JAMA* 293:987–997.
27. Travis WD, et al. (2002) *Non-Neoplastic Disorders of the Lower Respiratory Tract* (American Registry of Pathology and the Armed Forces Institute of Pathology, Washington, DC).
28. Mulder J, Hers JFP (1972) *Influenza* (Wolters-Noordhoff Publishing, Groningen), p 287.
29. Taubenberger JK, Morens DM (2008) The pathology of influenza virus infections. *Annu Rev Pathol* 3:499–522.
30. Winternitz MC, Wason IM, McNamara FP (1920) *The Pathology of Influenza* (Yale University Press, New Haven).
31. Stevens J, et al. (2006) Glycan microarray analysis of the hemagglutinins from modern and pandemic influenza viruses reveals different receptor specificities. *J Mol Biol* 355: 1143–1155.
32. Srinivasan A, et al. (2008) Quantitative biochemical rationale for differences in transmissibility of 1918 pandemic influenza A viruses. *Proc Natl Acad Sci USA* 105: 2800–2805.
33. Gill JR, et al. (2010) Pulmonary pathologic findings of fatal 2009 pandemic influenza A/H1N1 viral infections. *Arch Pathol Lab Med* 134:235–243.
34. Matrosovich MN, et al. (1997) Avian influenza A viruses differ from human viruses by recognition of sialyloligosaccharides and gangliosides and by a higher conservation of the HA receptor-binding site. *Virology* 233:224–234.
35. Reid AH, et al. (2003) 1918 influenza pandemic caused by highly conserved viruses with two receptor-binding variants. *Emerg Infect Dis* 9:1249–1253.
36. Jordan EO (1927) *Epidemic Influenza: A Survey* (American Medical Association, Chicago).
37. Andreasen V, Viboud C, Simonsen L (2008) Epidemiologic characterization of the 1918 influenza pandemic summer wave in Copenhagen: Implications for pandemic control strategies. *J Infect Dis* 197:270–278.
38. Anderson RM (1982) Directly transmitted viral and bacterial infections in man. *The Population Dynamics of Infectious Diseases*, ed Anderson RM (Chapman and Hall, Ltd, London), pp 1–37.
39. Wallinga J, Lipsitch M (2007) How generation intervals shape the relationship between growth rates and reproductive numbers. *Proc Biol Sci* 274:599–604.
40. Morens DM, Taubenberger JK (2011) Pandemic influenza: Certain uncertainties. *Rev Med Virol* 21:262–284.
41. Lowen AC, Mubareka S, Steel J, Palese P (2007) Influenza virus transmission is dependent on relative humidity and temperature. *PLoS Pathog* 3:1470–1476.
42. Shaman J, Kohn M (2009) Absolute humidity modulates influenza survival, transmission, and seasonality. *Proc Natl Acad Sci USA* 106:3243–3248.
43. Morens DM, Taubenberger JK, Fauci AS (2008) Predominant role of bacterial pneumonia as a cause of death in pandemic influenza: Implications for pandemic influenza preparedness. *J Infect Dis* 198:962–970.
44. Stevens J, et al. (2004) Structure of the uncleaved human H1 hemagglutinin from the extinct 1918 influenza virus. *Science* 303:1866–1870.
45. Brownlee GG, Fodor E (2001) The predicted antigenicity of the haemagglutinin of the 1918 Spanish influenza pandemic suggests an avian origin. *Philos Trans R Soc Lond B Biol Sci* 356:1871–1876.
46. Lowen A, Palese P (2009) Transmission of influenza virus in temperate zones is predominantly by aerosol, in the tropics by contact: A hypothesis. *PLoS Curr* 1:RRN1002.
47. Glaser L, et al. (2005) A single amino acid substitution in 1918 influenza virus hemagglutinin changes receptor binding specificity. *J Virol* 79:11533–11536.
48. Chan PK, et al. (2011) Clinical and virological course of infection with haemagglutinin D222G mutant strain of 2009 pandemic influenza A (H1N1) virus. *J Clin Virol* 50: 320–324.
49. Xu D, et al. (2009) Distinct glycan topology for avian and human sialopentasaccharide receptor analogues upon binding different hemagglutinins: A molecular dynamics perspective. *J Mol Biol* 387:465–491.
50. Nayak DP, Balogun RA, Yamada H, Zhou ZH, Barman S (2009) Influenza virus morphogenesis and budding. *Virus Res* 143:147–161.
51. Runstadler JA, et al. (2007) Using RRT-PCR analysis and virus isolation to determine the prevalence of avian influenza virus infections in ducks at Minto Flats State Game Refuge, Alaska, during August 2005. *Arch Virol* 152:1901–1910.
52. Sheng ZM, Chertow DS, Morens DM, Taubenberger JK (2010) Fatal 1918 pneumonia case complicated by erythrocyte sickling. *Emerg Infect Dis* 16:2000–2001.